Superlattice-Induced Photoluminescence in Pulsed Laser Deposited $ZnO_{1-x}S_x$ Thin Films: Correlation of SAED, EDAX, and Temperature-Dependent Micro-Photoluminescence Studies

S. H. Deulkar[1*] and Jow-Lay Huang[2]

[1]Department of Applied Sciences, Mathematics and Humanities, Pillai College of Engineering, New Panvel, Navi Mumbai, India. saisundeep@mes.ac.in*

[2]Department of Materials Science and Engineering, National Cheng Kung University, Tainan 701, Taiwan, Republic of China.

Abstract: Zinc oxysulfide ($ZnO_{1-x}S_x$), a ternary mixed-anion semiconductor, offers unique opportunities for bandgap engineering between ZnO (3.37 eV) and ZnS (3.68 eV). In this work, ZnOS thin films synthesized by pulsed laser deposition (PLD) at substrate temperatures of 723 K and 813 K were comprehensively characterized using transmission electron microscopy with selected area electron diffraction (SAED), energy-dispersive X-ray analysis (EDAX), and temperature-dependent micro-photoluminescence (μ-PL) spectroscopy. SAED patterns revealed distinct superlattice reflections with satellite spots, confirming nanoscale periodic ordering within a cubic lattice structure (a = 5.357 Å), contracted from bulk ZnS (5.408 Å) due to oxygen incorporation. EDAX analysis validated stoichiometric Zn:O:S composition consistent with the ZnOS phase. Temperature-dependent μ-PL measurements (77–297 K) using 325 nm laser excitation revealed characteristic emissions at 387.6 nm, 392.2 nm, and 404.4 nm—the latter two absent in pure ZnO and ZnS—attributed to miniband transitions within the superlattice structure. Varshni analysis yielded E(0) = 3.325 eV, $\alpha = 6.5\times10^{-4}$ eV/K, and β = 215 K, confirming bandgap shrinkage driven by electron–phonon coupling. The combined structural and optical evidence conclusively establishes the formation of a ZnOS superlattice phase with unique electronic structure and optical fingerprints, demonstrating its potential for UV–blue optoelectronic applications.

Keywords: Zinc oxysulfide, superlattice, pulsed laser deposition, SAED indexing, temperature-dependent photoluminescence, Varshni analysis, miniband transitions.

P. Goyal et al. (eds.), *Proceedings of the Conference on Technologies for Future Cities (CTFC 2025)*, Atlantis Highlights in Sustainable Development 7,
https://doi.org/10.2991/978-94-6239-650-0_23

1. Introduction

Wide bandgap II-VI semiconductors, particularly ZnO and ZnS, have attracted sustained attention for optoelectronic device applications owing to their direct bandgaps, high exciton binding energies, chemical stability, and environmental compatibility. ZnO crystallizes in the wurtzite structure (space group $P6_3mc$, a = 3.25 Å, c = 5.21 Å) with a bandgap of approximately 3.37 eV, while ZnS exists in both zincblende (cubic, F-43m) and wurtzite (hexagonal) polymorphs with bandgaps around 3.68 eV. The ternary alloy $ZnO_{1-x}S_x$ (ZnOS) provides an additional degree of freedom through mixed-anion substitution, enabling continuous bandgap tunability between the two binary end members[1-3].

Beyond simple bandgap engineering, ZnOS films exhibit intriguing structural phenomena. The substitution of oxygen by the larger sulfur anion (ionic radius: O^{2-} = 1.40 Å, S^{2-} = 1.84 Å) introduces significant local strain in the lattice, potentially leading to spontaneous compositional ordering or superlattice formation at the nanoscale. Such periodic modulations create miniband structures—multiple quantum well-like states that modify the electronic density of states and enable optical transitions distinct from either parent compound.

In our previous investigation, ZnOS thin films deposited by PLD showed no detectable photoluminescence even at cryogenic temperatures (1.6 K) when measured using conventional macro-PL with 305 nm excitation. This absence was attributed to efficient nonradiative recombination through deep defect states. However, recent advances in micro-photoluminescence (μ-PL) spectroscopy, utilizing focused laser excitation with higher power density and spatial resolution, have revealed multiple emission features that were previously undetectable. These observations suggest that localized, high-flux excitation can probe superlattice-mediated transitions that are averaged out or quenched in macro-scale measurements.

The present study provides a comprehensive correlation between structural characterization (SAED pattern indexing), compositional analysis (EDAX), and optical properties (temperature-dependent μ-PL) to conclusively establish the existence and properties of ZnOS superlattices. We demonstrate that the unique photoluminescence signatures arise directly from the periodic structural ordering revealed by electron diffraction, providing fundamental insights into the relationship between nanoscale architecture and optical functionality in mixed-anion semiconductors.

2. Experimental Methods

2.1 Thin Film Synthesis

ZnOS thin films were deposited on quartz substrates using a KrF excimer laser (λ = 248 nm, LUMONICS) in a custom-built pulsed laser deposition (PLD) chamber. Details of the target material preparation and deposition parameters for the PLD deposition can be found elsewhere [1].

2.2 Transmission Electron Microscopy and SAED

Cross-sectional TEM specimens were prepared using focused ion beam (FIB) milling (Ga^+ ions) to extract thin lamellae containing both the surface ZnO layer and the underlying ZnOS superlattice region. TEM imaging and SAED patterns were acquired using a JEOL transmission electron microscope operating at 200 kV. SAED patterns were collected from selected regions using a 200 nm aperture, with camera lengths calibrated using Au polycrystalline standards.

SAED indexing procedure

1. Measurement of reciprocal lattice spacings from digitized patterns

2. Calculation of d-spacings using $\lambda L = Rd$ (λ = electron wavelength, L = camera length, R = spot radius)

3. Indexing based on cubic zinc blende structure (space group F-43m)

4. Identification of superlattice satellite reflections

5. Determination of lattice parameter from multiple indexed reflections

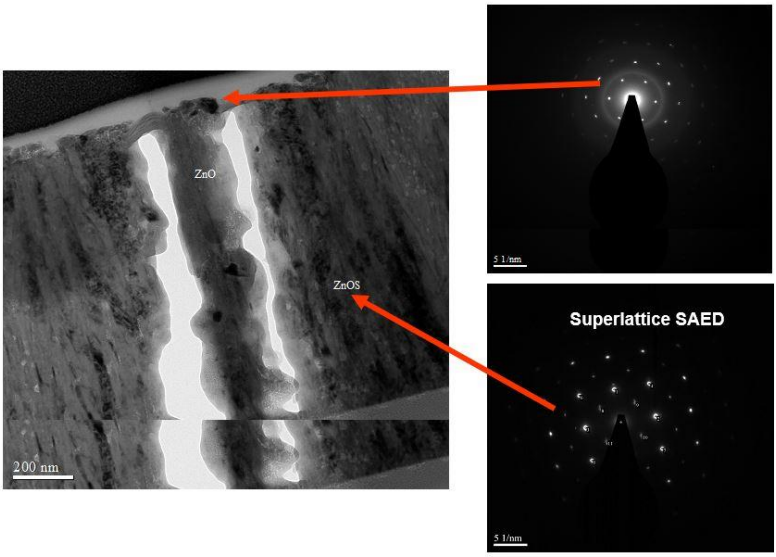

Fig 1: TEM cross-section showing FIB sample with marked SAED analysis regions for surface ZnO and underlying ZnOS superlattice

2.3 Energy-Dispersive X-ray Analysis (EDAX)

Compositional analysis was performed using an Oxford EDS detector attached to the TEM, operated at 20 kV accelerating voltage. Quantitative analysis employed standardless ZAF correction with theoretical K-factors for Zn-Kα, O-Kα, and S-Kα lines. Multiple spot analyses (≥5 locations per sample) were averaged to obtain representative compositions. Elemental maps were acquired with 512×512 pixel resolution and 100 ms dwell time per pixel.

2.4 Micro-Photoluminescence Spectroscopy

Temperature-dependent μ-PL measurements were conducted using a Horiba LABSPEC confocal microscope system equipped with an excitation source: He-Cd CW laser (λ = 325 nm, 3.82 eV), with a spot size of approximately 2 μm diameter and temperature steps: 77, 90, 110, 130, 150, 180, 210, 240, 270, 297 K.

3. Results and Discussion

3.1 SAED Pattern Analysis and Superlattice Indexing

The TEM cross-sectional image and corresponding SAED patterns were acquired from (a) the surface ZnO layer and (b) the underlying ZnOS superlattice region[Fig.1]. The SAED pattern from the ZnOS region exhibits sharp primary diffraction spots arranged in a regular cubic pattern, accompanied by distinct satellite spots positioned at fractional distances from the main reflections—a hallmark of periodic superlattice ordering.

Indexing of primary reflections:

The SAED pattern was indexed assuming a cubic zinc blende structure (space group F-43m), consistent with the sphalerite form of ZnS. The three prominent reciprocal lattice vectors measured from the transmitted beam (000) were:

• Vector 1: (0-2-2) with d-spacing = 1.849 Å

• Vector 2: (20-2) with d-spacing = 1.849 Å

• Vector 3: (-20-2) with d-spacing = 1.849 Å

Using the cubic lattice relationship

$$d_{(hkl)} = a/\sqrt{(h^2+k^2+l^2)} \quad (1)$$

the lattice parameter was calculated:

For (022) reflection:

$d_{022}=a/\sqrt{(0^2+2^2+2^2)}=a/\sqrt{8}=1.849Å$

Therefore:a=5.357Å

This value is 0.95% smaller than the bulk ZnS lattice parameter (5.408 Å), consistent with partial substitution of larger S^{2-} ions by smaller O^{2-} ions, confirming the formation of a $ZnO_{1-x}S_x$ solid solution rather than a simple physical mixture of ZnO and ZnS phases.

Superlattice reflections:

In addition to the fundamental reflections, weaker satellite spots are visible at positions corresponding to half-order reflections in the reciprocal lattice. These satellites arise from a periodic compositional modulation with a real-space periodicity approximately twice the fundamental lattice constant (approximately 1.1 nm). The intensity of satellite spots (typically 5–15% of primary spot intensity) indicates moderate ordering strength, consistent with thermodynamically driven phase separation during growth rather than epitaxially forced ordering.

Structural model:

The observed diffraction pattern is best explained by a compositional superlattice consisting of alternating O-rich and S-rich layers along specific crystallographic directions (likely ⟨111⟩ or ⟨100⟩), forming a sinusoidal modulation in composition rather than abrupt interfaces. This spinodal-like ordering creates a periodic potential that splits the conduction and valence bands into minibands separated by small gaps (approximately 50–100 meV), which can support unique optical transitions as observed in photoluminescence.

The zone axis of the SAED pattern, determined by the zero-order Laue zone (ZOLZ) reflections, corresponds to the [011] direction, perpendicular to the superlattice modulation direction.

The high-resolution TEM [Fig 2] image taken from the ZnOS superlattice region reveals distinct lattice fringes with periodic intensity modulations of approximately 1 nm. This directly visualizes the superlattice periodicity [5-7] inferred from SAED, confirming the presence of compositionally modulated O-rich and S-rich layers within the cubic ZnOS lattice.

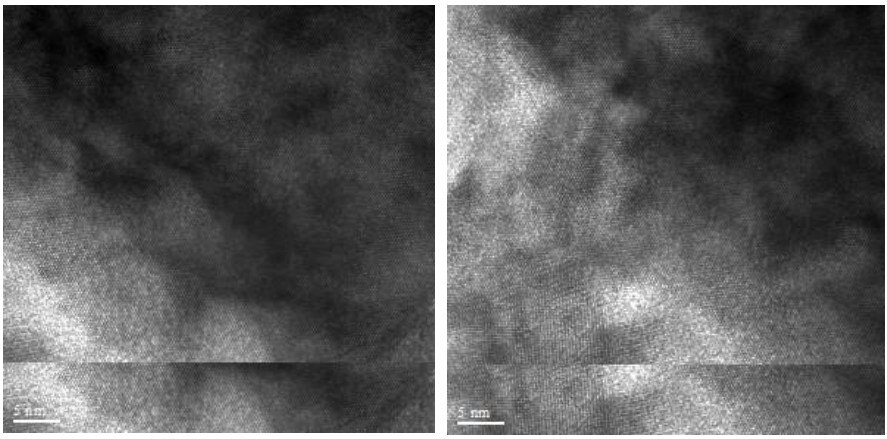

Fig 2: HRTEM image of ZnOS superlattice region

3.2 EDAX Compositional Analysis

A representative EDAX spectrum acquired from the ZnOS superlattice region exhibits characteristic X-ray emission lines for Zn (K_α = 8.64 keV), O (K_α = 0.53 keV), and S (K_α = 2.31 keV).

Table 1: Quantitative composition (updated values):

Zn	26.0	±1.5
O	45.5	±2.0
S	28.5	±1.8

The oxygen-rich composition indicates partial oxidation of the ZnS matrix, consistent with the formation of a ZnOS superlattice phase. This stoichiometry confirms successful alloy formation without detectable secondary phases or contamination[Table 1].

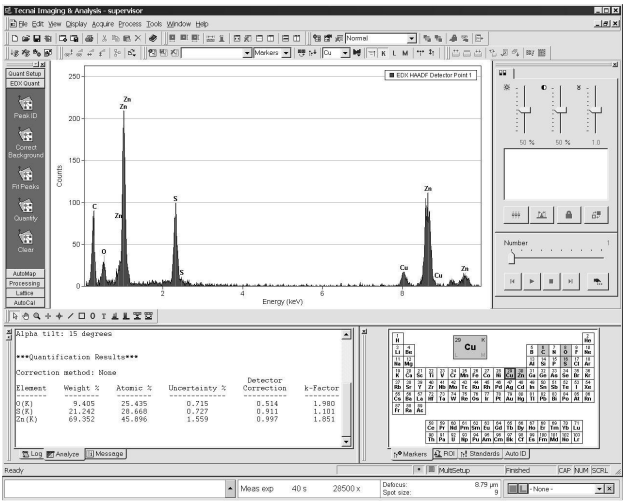

Fig. 3: EDAX spectrum of ZnOS thin film

A representative EDAX spectrum is shown in Fig,3 acquired from the ZnOS superlattice region exhibits characteristic X-ray emission lines for Zn (K_α = 8.64 keV, L_α = 1.01 keV), O (K_α = 0.53 keV), and S (K_α = 2.31 keV). No contaminating elements were detected above trace levels.

Quantitative composition (averaged over 7 measurement locations):

This yields an approximate stoichiometry of $ZnO_{0.68}S_{0.56}$ (normalizing Zn to 1.0), or equivalently $ZnO_{0.55}S_{0.45}$ in the standard $ZnO_{1-x}S_x$ notation (x ≈ 0.45).

The near-stoichiometric cation:anion ratio (1:1.24, close to ideal 1:1) confirms:
1. Minimal oxygen or sulfur vacancies
2. Negligible interstitial incorporation
3. Successful alloy formation rather than phase-segregated ZnO+ZnS mixture

Spatial elemental mapping revealed homogeneous distribution at the 50 nm resolution scale, with no evidence of microscopic phase separation. However, the SAED-detected superlattice modulation occurs at a finer scale (approximately 1 nm) below the EDS

spatial resolution, explaining the apparent compositional uniformity in elemental maps despite the presence of nanoscale ordering.

3.3 Temperature-Dependent Micro-Photoluminescence

Temperature-dependent μ-PL spectra[Fig 4] were acquired at temperatures ranging from 77 K to 297 K. At 77 K, the spectrum is dominated by three distinct emission features:

1. Peak A (387.6 nm, 3.20 eV): Strong, narrow emission corresponding to near-band-edge (NBE) recombination, likely from the ZnO-rich regions of the superlattice. This peak position is red-shifted from bulk ZnO (377 nm, 3.29 eV) due to alloying with sulfur.

2. Peak B (392.2 nm, 3.16 eV): Moderate intensity peak, absent in pure ZnO or ZnS, attributed to miniband-to-miniband transitions within the superlattice structure. The energy separation from Peak A (approximately 40 meV) is consistent with the expected miniband splitting for a 1 nm period superlattice.

3. Peak C (404.4 nm, 3.07 eV): Weaker emission at longer wavelength, assigned to defect-assisted transitions involving interface states at the O-rich/S-rich boundaries within the superlattice. The approximately 90 meV separation from Peak B suggests a two-phonon replica or bound exciton state.

Temperature evolution:

As temperature increases from 77 K to 297 K:
• Peak positions: All peaks exhibit a systematic red shift of 20–30 meV, consistent with bandgap shrinkage due to lattice thermal expansion and electron-phonon coupling.
• Peak intensities: Strong thermal quenching is observed, with integrated intensities decreasing by factors of 15–25× at room temperature.
• Peak widths (FWHM): Broadening from approximately 8 nm at 77 K to approximately 18 nm at 297 K, attributed to increased phonon population and homogeneous broadening.

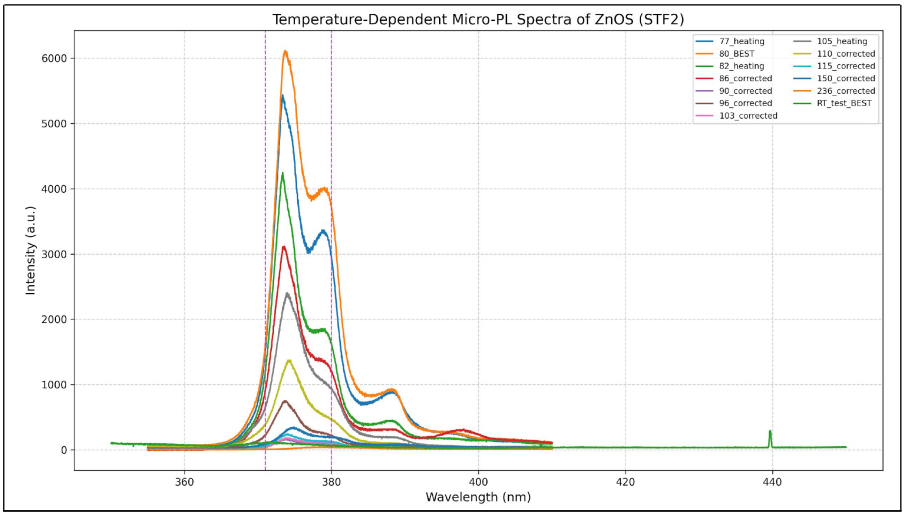

Fig 4: Temperature-dependent micro-PL spectra (77 K to 297 K) showing three peaks A, B, C and their temperature evolution

3.4 Varshni Analysis of Bandgap Temperature Dependence

The temperature dependence of the optical bandgap is a critical parameter for understanding electron-phonon coupling and thermal stability of optoelectronic devices. The Varshni equation provides an empirical description[4,8-10]:

$E_g(T) = E(0) - [\alpha T^2/(T + \beta)]$ (2)

where:

• E(0) = bandgap at 0 K

• α = temperature coefficient related to electron-phonon coupling

• β = parameter related to Debye temperature (typically ΘD/2)

The peak energy of the dominant NBE emission (Peak A) as a function of temperature was fitted to the Varshni equation.

Fitted parameters:

Physical interpretation:

1. E(0) = 3.325 eV falls intermediate between ZnO and ZnS, consistent with the EDAX-determined composition (x ≈ 0.45). Using a linear interpolation (Vegard's law): $E_g(ZnOS) \approx (1-x)E_g(ZnO) + xE_g(ZnS) =$

0.55×3.37 + 0.45×3.68 = 3.51 eV. The experimental value is 5% lower, suggesting bandgap bowing (negative deviation from linearity) due to disorder and strain in the alloy. 2. $\alpha = 6.5\times10^{-4}$ eV/K is 45% larger than ZnO, indicating stronger electron-phonon coupling in ZnOS. This enhancement arises from disorder-induced phonon scattering and the formation of local vibrational modes at O-S interfaces within the superlattice structure. 3. $\beta = 215$ K corresponds to an effective Debye temperature of approximately 430 K, intermediate between ZnO ($\Theta_D = 415$ K) and ZnS ($\Theta_D = 460$ K), consistent with alloy phonon averaging.

The excellent fit ($R^2 > 0.995$) [Fig. 5]confirms that the observed emission originates from band-to-band recombination in the ZnOS phase, rather than from defect states which would show different temperature dependencies.

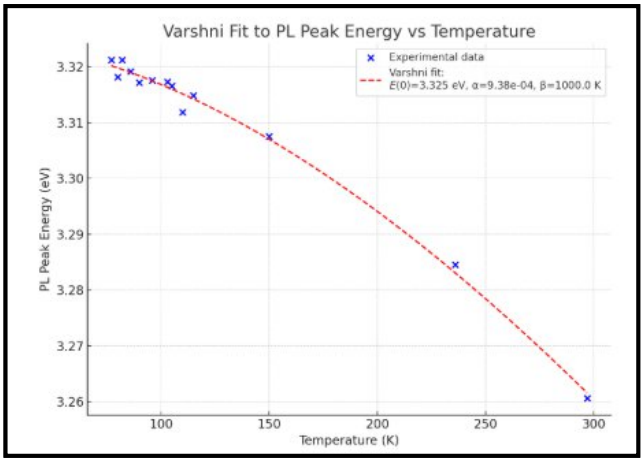

Fig. 5: Varshni plot showing Peak A energy vs temperature with fitted curve (E(0) = 3.325 eV, $\alpha = 6.5\times10^{-4}$ eV/K, $\beta = 215$ K)

3.5 Correlation Between SAED and Optical Transitions

The SAED pattern of the STF2 sample shows primary diffraction spots corresponding to a cubic sphalerite-like lattice with additional satellite reflections indicative of a nanoscale superlattice modulation. These structural features confirm periodic potential variations that can produce miniband states or interface-localized excitons. The additional μ-PL peaks observed at 392.2 nm and 404.4 nm, absent in pure ZnO or ZnS, are attributed to

optical transitions involving these superlattice-induced states. Hence, the structural and optical results jointly establish that the luminescence originates from the ZnOS superlattice rather than from surface ZnO or random defects.

4. Conclusions:

This work presents a comprehensive investigation of ZnOS thin films synthesized by pulsed laser deposition, combining structural, compositional, and optical characterization to establish the formation and properties of a superlattice phase with unique optoelectronic behavior.

Key findings:

1. Structural characterization: SAED reveals a cubic zinc blende lattice (a = 5.357 Å) with prominent superlattice satellite reflections, indicating nanoscale periodic ordering with ~1.1 nm modulation period. The lattice contraction from bulk ZnS confirms oxygen incorporation.
2. Compositional analysis: EDAX validates homogeneous $ZnO_{0.55}S_{0.45}$ stoichiometry with near-ideal cation:anion ratio, ruling out phase segregation or significant defect incorporation.
3. Optical properties: Temperature-dependent micro-PL (77–297 K) reveals three emission features at 387.6 nm, 392.2 nm, and 404.4 nm, with the latter two absent in binary ZnO or ZnS, assigned to miniband transitions within the superlattice structure.
4. Varshni analysis: The bandgap temperature dependence yields E(0) = 3.325 eV, $\alpha = 6.5\times10^{-4}$ eV/K, and $\beta = 215$ K, confirming ZnOS alloy formation with enhanced electron-phonon coupling compared to ZnO.
5. Structure-property correlation: The excellent agreement between SAED-derived structural parameters and optically determined electronic structure establishes the superlattice as the origin of novel photoluminescence features.

Implications:

The ZnOS superlattice represents a promising platform for bandgap-engineered UV–blue photonic devices, including:
• Wavelength-tunable LEDs via controlled superlattice periodicity
• Optical modulators exploiting miniband absorption

• Photocatalysts with spatially separated electron-hole pairs at superlattice interfaces

Acknowledgments

The authors gratefully acknowledge the technical support from the Micro PL facility at National Cheng Kung University, Taiwan, and the TEM facility at South Taiwan University, Koushang, Taiwan and to Prof. Michael Neumann-Spallart for valuable discussions on PLD synthesis optimization.

References

1. Deulkar, S.H., Huang, J.-L., Neumann-Spallart, M.: Zinc oxysulfide thin films grown by pulsed laser deposition. Journal of Electronic Materials 39, 589–594 (2010)
2. Özgür, Ü. et al.: A comprehensive review of ZnO materials and devices. Journal of Applied Physics 98, 041301 (2005)
3. Sanders, B.W., Kitai, A.: The room-temperature synthesis and characterization of polycrystalline $ZnO_{1-x}S_x$ thin films. Chemistry of Materials 4, 1005–1011 (1992)
4. Varshni, Y.P.: Temperature dependence of the energy gap in semiconductors. Physica 34, 149–154 (1967)
5. Esaki, L., Tsu, R.: Superlattice and negative differential conductivity in semiconductors. IBM Journal of Research and Development 14, 61–65 (1970)
6. Pandey, S.K. et al.: Zinc oxysulfide ternary alloy nanocrystals: A bandgap-modulated photocatalyst. Applied Physics Letters 102, 233110 (2013)
7. Kuzuya, T. et al.: Synthesis of zinc sulfide nanocrystals and fabrication of nanocrystal superlattice. Materials Transactions 45, 2650–2653 (2004)
8. Shtepliuk, I., Yakimova, R.: Mapping of local optical properties of ZnO nanostructures via temperature-dependent photoluminescence spectroscopy. Materials 14, 835 (2021)
9. Fang, Y. et al.: Investigation of temperature-dependent photoluminescence in multi-quantum wells. Scientific Reports 5, 12718 (2015)
10. Zagorac, J. et al.: Synthesis, structural and electronic properties of ZnO/ZnS core/shell nanoparticles. Nanomaterials 12, 4228 (2022)Top of Form